Annu. Rev. Phys. Chem. 2001. 52:357–89

STRUCTURE AND BONDING OF MOLECULES AT AQUEOUS SURFACES

GL Richmond
Department of Chemistry, University of Oregon, Eugene, Oregon 97403;
e-mail: Richmond@oregon.uoregon.edu

Key Words vibrational spectroscopy, nonlinear optics, hydrogen bonding, water

■ **Abstract** Significant advances toward understanding the structure of aqueous surfaces on a molecular level have been made in recent years. This review focuses on the recent contributions of surface vibrational sum frequency spectroscopy (VSFS) to this field of study. An overview of recent VSFS studies of the molecular structure and orientation of molecules at the vapor-water interface and the interface between water and an immiscible organic liquid is presented, with particular emphasis on studies that compare the molecular properties and adsorbate behavior at these two different but related interfaces. This discussion is preceded by a general introduction to VSFS studies at aqueous surfaces and a description of the fundamental principles underlying the technique.

INTRODUCTION

Aqueous surfaces are central to our existence on this planet. The water-vapor interface provides a template for many reactive processes in the atmosphere and aqueous surfaces on the earth. Protein folding, membrane formation, and micellar assembly are a few of the many processes for which the interaction of water with a hydrophobic macromolecular surface is key. Ion or solute transport across a water-hydrophobic liquid interface relies upon the differing interactions between the transferring species and the water and organic solvent molecules in the interfacial region. Our understanding of interactions at water surfaces has largely been derived from theoretical efforts in the past several decades (1–12). This is particularly true for buried liquid interfaces such as the junction between two immiscible liquids or water-hydrating macromolecule and organic molecular assemblies (13–21). Recent advances in experimental methods that can probe aqueous surfaces with molecular specificity have made possible the first direct measurements of the molecular properties of water surfaces (22–38). These studies demonstrate the unique properties of liquid surfaces relative to solid surfaces. They also illustrate the complex interactions that are present at these interfaces, interactions that will require a combination of advanced experimental and theoretical approaches to

0066-426X/01/0601-0357$14.00

understand. However, the challenge is worth pursuing with vigor, given the key role that these surfaces play in chemical, physical, and biological processes.

One particularly promising method for studying liquid surfaces and interfaces is vibrational sum frequency spectroscopy (VSFS). This review provides an overview of some of the recent studies in which VSFS has been used to measure the molecular properties of vapor-water and organic-liquid-water interfaces. The review begins with a description of VSFS, including examples of optical systems used for VSFS measurements. Information gained from selected studies in this field is then described, beginning with studies on the structure and hydrogen bonding of interfacial water molecules. This is followed by a summary of studies that examine how interfacial water is perturbed by the presence of surfactants and adsorbates. The remaining portion of the review focuses on studies of adsorbate structure and conformation measured at both types of interfaces. This review places particular emphasis on recent findings concerning the similarities and differences in the behavior of molecules at aqueous vapor-liquid and aqueous liquid/hydrophobic liquid interfaces. The comparison provides some fascinating new insights about differences in hydrogen bonding of water and the assembly of monolayers at these two interfaces.

VIBRATIONAL SUM FREQUENCY SPECTROSCOPY

Theoretical Considerations

VSFS is a second-order nonlinear optical process that directly measures the vibrational spectrum of molecules at an interface. Pioneered by Shen in the mid 1980s (39), this technique is uniquely suited for surface studies because of its inherent surface sensitivity. Under the dipole approximation, this second-order process is forbidden in media that possess inversion symmetry (40, 41). At the interface between two centrosymmetric media there is no inversion center and thus vibrational sum frequency (VSF) is allowed in the interfacial region. Consequently, the asymmetric nature of interfaces allows a regional selectivity to interfacial properties on a molecular level that is not inherent to other linear surface vibrational spectroscopies.

In a VSFS experiment, a visible laser beam and a tunable IR laser beam are coincident at the interface. The energy range of the tunable IR laser is chosen to overlap with the energies of vibrational modes of molecules present at the interface. By scanning the energy of the IR laser and monitoring the generated sum frequency (SF) signal, a vibrational spectrum of the interfacial molecules can be measured. The VSFS intensity is proportional to the square of the surface nonlinear susceptibility $\chi_s^{(2)}(\omega_{sfg} = \omega_{vis} + \omega_{ir})$ as

$$I_{sfg} \propto |P_{sfg}|^2 \propto \left| \chi_{NR}^{(2)} + \sum_{\nu} |\chi_{R_\nu}^{(2)}| e^{i\gamma_\nu} \right|^2 I_{vis} I_{ir}, \qquad 1.$$

where P_{sfg} is the nonlinear polarization at ω_{sfg}; χ_{NR} and χ_{R_ν} are the nonresonant and resonant parts of $\chi_s^{(2)}$, respectively; γ_ν is the relative phase of the νth vibrational mode; and $I_{\nu is}$ and I_{ir} are the visible and IR intensities, respectively. Because the susceptibility is generally complex, the resonant terms in the summation are associated with a relative phase γ_ν, which is used to account for any interference between two modes that overlap in energy. $\chi_{R_\nu}^{(2)}$ is also proportional to the number density of molecules, N, and the orientationally averaged molecular hyperpolarizability, β_ν, as follows:

$$\chi_{R_\nu}^{(2)} = \frac{N}{\varepsilon_0}\langle\beta_\nu\rangle. \qquad 2.$$

Thus the square root of the measured SF intensity is proportional to the number density of molecules at the surface or interface. The molecular hyperpolarizability, β_ν, is enhanced when the frequency of the IR field is resonant with a SF-active vibrational mode of a molecule at the surface or interface. This enhancement in β_ν leads to an enhancement in the nonlinear susceptibility $\chi_{R_\nu}^{(2)}$, which can be expressed as

$$\chi_{R_\nu}^{(2)} \propto \frac{A_\nu}{\omega_\nu - \omega_{ir} - i\Gamma_\nu}, \qquad 3.$$

where A_ν is the intensity of the νth mode and is proportional to the product of the Raman and IR transition moments, ω_ν is the resonant frequency, and Γ_ν is the line width of the transition. Because the intensity term, A_ν, is proportional to both the IR and Raman transition moments, only vibrational modes that are both IR and Raman active will be SF active. Molecules or vibrational modes that possess an inversion center will not be SF active.

The surface susceptibility $\chi_s^{(2)}$ in general is a 27-element tensor. It can often be reduced to several nonvanishing elements by invoking symmetry constraints. Liquid surfaces and interfaces of liquid surfaces are isotropic in the plane of the surface. The symmetry constraints for an in-plane isotropic surface ($C_{\infty v}$) reduce $\chi_s^{(2)}$ down to the following four independent nonzero elements:

$$\chi_{zzz}^{(2)};\ \chi_{xxz}^{(2)} = \chi_{yyz}^{(2)};\ \chi_{xzx}^{(2)} = \chi_{yzy}^{(2)};\ \chi_{zxx}^{(2)} = \chi_{zyy}^{(2)}, \qquad 4.$$

where z is the direction normal to the surface. These four independent elements contribute to the VSFS signal under the four different polarization conditions, *SSP*, *SPS*, *PSS*, and *PPP* (explained below), which are listed in the order of decreasing frequency (SF, Vis, IR). Light polarized parallel to the incident plane is referred to as *P* polarization, whereas light polarized perpendicular to the incident plane is *S* polarized. Which vibrational modes contribute to a particular polarization combination depends on the polarization of the IR field and the direction of the IR and Raman transition moments. The *SSP* polarization combination accesses vibrational modes with dipole transition moments that have components perpendicular to the surface plane. *SPS* and *PSS* polarization combinations access modes that have transition moments with components parallel to the surface plane. The

intensity under *PPP* polarization conditions contains contributions from all of the tensor elements. Thus vibrational modes with components that are both perpendicular and parallel to the surface plane will be present in *PPP*-polarized VSFS spectra. *SSP* polarization has been used in most studies to date. *PSS* polarization has been used less frequently because of low signal levels for most liquid surfaces. Studies conducted with *SSP*, *SPS*, and *PPP* have been very useful in verifying peak assignments and orientation in VSFS (38).

Experimental Considerations

As mentioned above, VSFS involves overlapping two pulsed laser beams at the surface, one of fixed frequency in the visible and another of variable frequency in the IR spectrum. The SF process at liquid surfaces is very weak, so pulsed lasers are necessary to attain detectable SF signals. Because the SF signal increases with peak intensity, shorter pulses (i.e. picosecond or femtosecond) are optimal, although shorter pulses translate into broader IR bandwidths. Nanosecond lasers are often easier to operate and have narrower bandwidths but can lead to unwanted heating unless an optical coupling scheme such as total internal reflection (TIR) (38) or other mechanisms such as rotation of the sample (29) are used.

Most VSF studies to date have focused in IR regions where nanosecond and picosecond lasers operate with the highest power densities, for example, in the 3-μm region. IR light has been produced by a number of optical parametric processes, such as generation (OPG), oscillation (OPO), and amplification (OPA) (38, 42) as well as difference frequency mixing (43) and stimulated Raman scattering (44). In our laboratory we use both nanosecond and picosecond systems. The nanosecond systems are used primarily for liquid-liquid studies with the light coupled to the interface in a TIR geometry to attain sensitivity levels comparable to picosecond laser studies (38). For such TIR studies, the incident beams are sent through the higher-index medium at the critical angle for each particular beam. The VSF response is collected in reflection at the corresponding critical angle for the SF signal. The enhancement in the SF response using this TIR geometry is several orders of magnitude higher than that obtained using an external reflection geometry. The nanosecond system relies upon the 1064-nm output of an injection-seeded neodymium: yttrium/aluminum/garnet laser to pump a potassium titanyl phosphate (KTP) OPO/OPA assembly. This system produces tunable IR from 2.5 μm (4000 cm^{-1}) to 5 μm (1975 cm^{-1}), with usable energies ranging from 4 mJ to 1 mJ at the two respective limits. It also operates at 1 cm^{-1} resolution and has a variable repetition rate (1–100 Hz). For air-liquid studies, a picosecond laser is used (42). This picosecond system produces 800-nm light (kilohertz repetition rate, 2 ps, 1.6 W) with a titanium:sapphire (Coherent Mira) passively mode-locked laser pumped with 5.5 W of 532-nm laser light from a Coherent Verdi laser. The 800-nm light used is temporally stretched, amplified with a Quantronix regenerative amplifier and double-pass titanium:sapphire amplifier, and recompressed. The IR light (2700–4000 cm^{-1}) is produced via a home-built optical parametric

amplifier pumped by the 800-nm light. This amplifier consists of two angle-tuned KTP crystals. Recent changes to this system over previous work (45) include the incorporation of a 2-cm-long MgO:$LiNbO_3$ crystal that is used as the optical parametric generator (OPG) from which the resultant 1- to 1.2-μm wavelengths are used to seed the KTP crystal. A grating for the selection of the seed wavelength is used. The IR light is generated by seeding the first KTP crystal and then amplifying it through the second KTP crystal. For the air-water studies, both beams are passed though a closed cell to minimize contamination. This system is currently being upgraded to produce IR as low as 8 μm.

Other variations on the traditional means of acquiring SF spectra in a scanning IR mode have recently appeared, both using femtosecond pulses. McGuire et al (46) have demonstrated a Fourier-transform spectroscopic technique based on VSFS. This method results in nearly unlimited spectral resolution and is based on Fourier transform of an SF-upconverted interferogram of an IR-induced polarization on the surface of the sample. Another method capitalizes on the variation of the SF exit angle with frequency, with the SF signal collected by different elements of a multielement detector (47). Here, the spectral resolution depends on the beam divergence. The third method simply disperses the broadband SF signal that is generated by femtosecond IR and narrow-band visible pulses by a monochromator and records the signal on a CCD camera (48).

HYDROGEN BONDING OF INTERFACIAL WATER

The unique properties of water surfaces have fascinated scientists for centuries. Strong hydrogen bonding between water molecules at a water surface is generally recognized to be responsible for the anomalously high surface tension present at the vapor/water interface (3). This section summarizes VSF measurements of the structure and hydrogen bonding of water molecules at both the vapor-water and organic-matter–water interfaces and discusses differences found in the behavior of water at these two interfaces. The summary includes recent developments in analysis of VSF spectral data of water. Results of a series of papers that have investigated the effect of different charged surfactants on the hydrogen bonding of water at both interfaces are also summarized. The section concludes with a description of vapor-water studies that are pertinent to important environmental issues.

Vibrational Sum Frequency Spectrum of the Vapor-Water Interface

The vibrational spectrum of water is of particular interest because hydrogen bond interactions are highly sensitive to the local molecular environment (3, 49–53). The vibrational spectrum of water therefore provides a sensitive probe of the structure and energetics of the hydrogen bond network at the water interface. The sensitivity of VSFS to surface water vibrational modes is accompanied by a complexity in

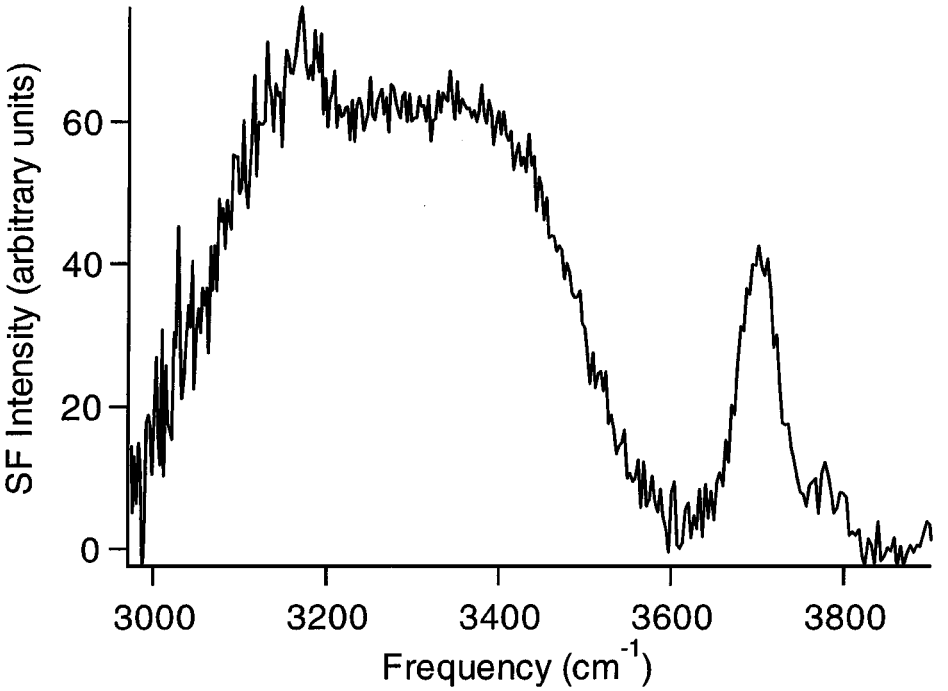

Figure 1 Vibrational sum frequency spectrum of the vapor/water interface using *SSP* polarization. A picosecond laser system described in the text was used. From LF Scatena & GL Richmond, submitted manuscript.

spectral interpretation that is only beginning to be explored by researchers in depth, owing to the variety of environments of the interfacial water molecules and various degrees of hydrogren bonding. This difficulty in interpretation is not unique to surface vibrational spectroscopy but has been a major point of controversy over past decades in the interpretation of bulk water spectra (52–54).

Du et al (55) reported the first VSF spectrum of the vapor-water interface. Figure 1 shows the VSF spectrum from this interface that was obtained in this laboratory (56, 57). The data have been taken with *SSP* polarization, which accesses vibrational modes that have components of their transition dipole in the plane perpendicular to the interface. The experiments were conducted in a purged cell as well as under ambient conditions. The spectra give identical results as long as the ambient experiments are conducted in such a way as to minimize any contamination problems. The 2-ps titanium:sapphire-based system described above was used. The spectrum shares the general features of earlier work of Du et al (55). Assignment of spectral features in this spectrum relies heavily on IR and Raman assignments of OH stretching modes taken from bulk water measurements. The surface water spectrum has the general shape of an isotropic Raman bulk water OH

spectrum, yet there are important differences. Consistent with Raman and IR pH data and cluster studies, the VSF intensity in the 2900 cm^{-1} region is attributed to the very strong symmetric hydrogen bonding found in various water cluster distributions (58). Cationic and anionic water species that tend to partition to an aqueous surface could also be contributing to this intensity (59, 60). The broad band from $\sim$3000 to 3600 cm^{-1} is assigned to the large distribution of OH hydrogen-bonding stretching modes in which the oxygen is tetrahedrally coordinated (49, 61–64). The energy region from $\sim$3000 to 3250 cm^{-1} is attributed to strong intermolecular in-phase hydrogen bonds of water molecules that give rise to a highly correlated hydrogen-bonding network. This region is dominated by a continuum of OH symmetric stretches, ν_1. The higher-energy broadband region ($\sim$3250 to 3500 cm^{-1}) is assigned to more weakly correlated hydrogen-bonded stretching modes of molecular water that encompass both ν_1 (OH symmetric stretch) and, to a lesser extent, ν_3 (OH asymmetric stretch) vibrational modes. The distinct peak at 3702 cm^{-1} is assigned to the dangling OH bond of interfacial water molecules that straddle the interface. This bond projects into the vapor phase. The relatively high energy of this mode reflects its intramolecular uncoupling with the other OH bond in the molecule, the donor bond. The donor bond is expected to appear at lower energies owing to its interactions in the surface plane with other interfacial water molecules. Interactions with the free OH bond mode are largely through the oxygen atom. Spectral corrections for the dispersion in the Fresnel coefficients and normalization in the SF response for a nonresonant substrate are not shown. When these corrections are made, there is minimal change in the spectrum except to enhance the intensity of the free OH mode relative to the broad hydrogen-bonded peaks. Schnitzer et al (65), Simonelli et al (66), and Schnitzer et al (67) have made similar measurements of the air/water spectrum using a nanosecond system rather than the picosecond laser systems used in the work by Allen et al (68) and Du et al (22). Schnitzer et al and Simonelli et al observed the free OH peak and a broad distribution of OH modes in the 3000–3500 cm^{-1} region, but their spectra also show an intensity drop to nearly zero around 3200 cm^{-1} (65–67).

Overall, the vapor-water interfaces suggest very strong hydrogen bonding at the surface. The strong intensity in the lower-energy region is consistent with a highly coordinated water structure, often referred to as "icelike" hydrogen bonding between water molecules because intensity in the 3200 cm^{-1} region is characteristic of IR peaks found in bulk ice. IR absorption in the 3400 cm^{-1} region of the spectrum is more characteristic of liquid water. Du et al (69) estimate that $\sim$20% of surface water molecules have one free OH projecting into the vapor phase.

Water Hydrogen Bonding at the Organic-Liquid/ Water Interface

The interfacial tension of an organic-liquid/water interface is known to decrease with the increased polarity of the organic phase until both phases are miscible. Most of what is known on a molecular level about water structure next to a hydrophobic

fluid or solid surface has come from theoretical efforts (13–21). The difficulty in accessing this interface with a technique that can selectively probe interfacial water is the reason that so few experimental studies have been conducted. Nearly all studies to date have used VSFS and, of these, most have been conducted at the CCl_4/H_2O interface (70–74).

The CCl_4/H_2O system has some attractive features that make it a model system for understanding the hydrogen bonding of water near a hydrophobic liquid. In addition to being largely immiscible in water, it has an interfacial tension (48 mN m^{-2}) similar to alkane/water ($\sim$51 mN m^{-2} for C_6–C_8). CCl_4 has a electric dipole polarizability that is nearly identical to alkanes such as *n*-hexane but does not have CH stretch vibrational modes that energetically overlap and complicate the spectral interpretation of the OH water modes used to study hydrogen bonding at interfaces.

Figure 2*a* shows the VSF spectra of water measured at the CCl_4/H_2O interface. The data are taken in a TIR optical geometry using the 3.5-ns neodymium: yttrium/aluminum/garnet-pumped laser system described above (LF Scatena & GL Richmond, submitted manuscript). Because the two experiments used different laser systems, peak positions in this spectrum and that for the vapor-water interface shown in Figure 1 can be compared, but only qualitative comparisons with peak intensities are appropriate. The most obvious difference between the two spectra is the remarkable shift in overall intensity to higher energies for CCl_4/H_2O, which is indicative of significantly weaker hydrogen bonding at this liquid-liquid interface. This observation is consistent with a much lower interfacial tension relative to air-water (71 mN m^{-2}). These VSF results for CCl_4/H_2O are a refinement on earlier work for water at this interface (75) in which the dangling bond OH mode (free OH) could not be probed because of laser limitations. These later results were obtained in a special cell designed to minimize solvent volume.

The weaker nature of the hydrogen bonding at this interface has facilitated assignment of spectral features in the CCl_4/H_2O spectrum. The free-OH mode for water is clearly apparent at the CCl_4/H_2O interface, but its energy is red shifted (3662 ± 1 cm^{-1}) relative to the vapor-water interface (3702 cm^{-1}) (55–57). From studies of HOD monomers in CCl_4, LF Scatena & GL Richmond (submitted manuscript) have determined that this red shift is the result of an attractive interaction between the dangling OH bond and the surrounding CCl_4 molecules. The binding energy for the H_2O-CCl_4 complex is reported to be -1.4 kcal mol^{-1} (76, 77). (This mode is therefore referred to as the dangling bond mode because it is not as free as in the vapor phase.) The results are consistent with previous simulations of this interface that suggest a locally sharp transition between phases (13, 21). VSF studies of HOD at this interface provide further assignments. In addition to the OH dangling bond and OD dangling bond of HOD at the interface (measured at 3664 cm^{-1} and 2712 cm^{-1}, respectively), a broader peak is observed near 3450 cm^{-1} that is attributed to the donor OH mode of the water molecules that straddle the interface. Because intensity is detected with I_{SSP} polarization, this H-bonded mode, which is largely uncoupled from the OH dangling-bond mode

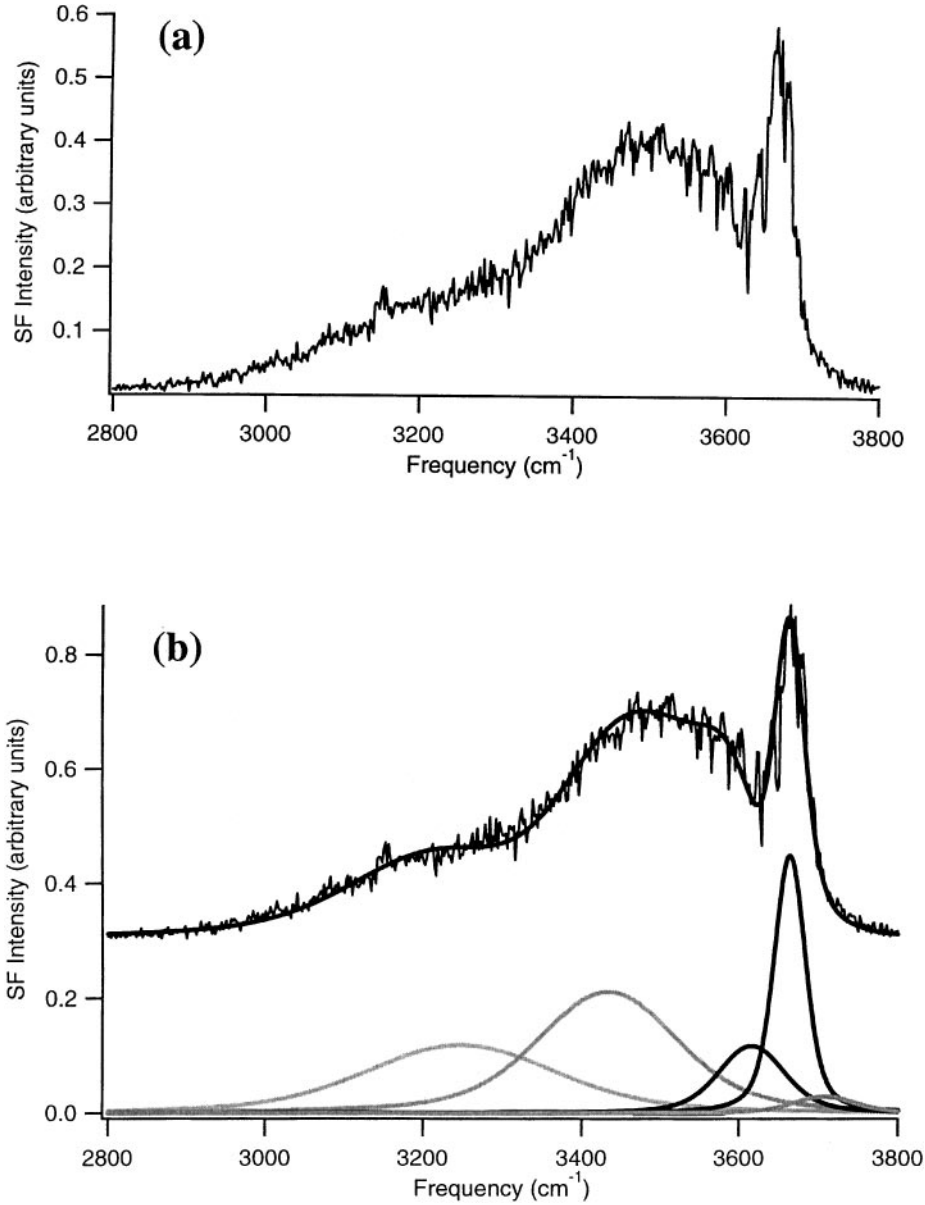

Figure 2 (*a*) Vibrational sum frequency spectrum of the CCl_4/H_2O interface using the 1-ns laser system described in the text (LF Scatena & GL Richmond, submitted manuscript). The spectra were collected in a total internal reflection geometry with *SSP* polarization used. This spectrum was achieved without the trace impurities that were apparent in the previously published spectra (75). (*b*) Spectral analysis of the CCl_4/H_2O interface using the procedures outlined in the text. The upper curve shows the spectral fit; the lower curves show contributions from each of the vibrational modes. The gray peaks have a phase opposite to that of the black peaks, as determined from fits to the data using Voigt profiles. Published with permission from Reference 57.

in the molecule, does not lie exactly in-the-plane of the interface but has some perpendicular component.

The remaining portion of the H_2O spectrum of Figure 2*a* between 3450 and 3700 cm^{-1} is attributed to weakly interacting water molecules in the interfacial region, such as water monomers (LF Scatena & GL Richmond, submitted manuscript). The OH stretch of water monomers in bulk CCl_4 shows two characteristic IR peaks, one associated with the symmetric OH stretch (SS or ν_1) of water monomers (3616 cm^{-1}) and the other (3708 cm^{-1}) associated with the asymmetric OH stretch (AS or ν_3). These two peaks energetically bracket the dangling bond stretch mode in the VSF spectrum. Careful analysis (described below) of the data shows that both modes are present in the VSF spectrum, the SS and the AS of water monomers respectively, which constructively and destructively interfere with the neighboring dangling OH bond mode (57).

Overall, the results suggest that, unlike the air-water interface, the hydrogen bonding at the CCl_4/H_2O interface is very weak. Intensity is observed in the strongly hydrogen-bonded region (3200–3400 cm^{-1}), but overall the spectra are dominated by water species that have only weak interactions with other water molecules and CCl_4 molecules. This is the first spectroscopic evidence for the existence of water molecules at an oil-water interface that have the spectroscopic characteristics of water monomers in the organic phase.

Vibrational Sum Frequency Spectral Analysis of Interfacial H_2O

Obtaining spectral fits to VSF water spectra is difficult because of the wide range of contributing vibrational modes, the breadth of the spectral peaks for hydrogen-bonded water molecules, and the complex interference effects that can arise between adjacent vibrational modes. Because VSFS is a coherent nonlinear spectroscopic technique, each resonant vibrational mode has an inherent phase for a fixed orientation. Resonant modes that change phase with the orientation of the molecule may interfere constructively or destructively when overlapped in frequency. The most detailed analysis to date for water spectra has recently appeared (57). This analysis has been applied to the water-vapor and the CCl_4/H_2O data described above. The work considers a range of water species present at a water surface and the possible interference between these contributing modes, and it takes into account the phase of the SF response from contributing vibrational modes. This phase is useful in obtaining an average orientation of molecules at the surface by relating the macroscopic second-order susceptibility, $\chi^{(2)}$, of the system to the molecular hyperpolarizabilities, β_v, of the individual molecules at the interface (78, 79). The molecular hyperpolarizability is often described as

$$\beta_{\mathrm{lmn},\nu} = \frac{\langle g|\alpha_{lm}|\nu\rangle\langle\nu|\mu_n|g\rangle}{\omega_{\mathrm{IR}} - \omega_\nu + i\Gamma_\nu}, \qquad 4.$$

where *l*, *m*, and *n* represent the molecular inertial axes (a, b, and c); $\mu_{\rm n}$ and $\alpha_{\rm lm}$ represent the dipole and Raman vibrational transition moments, respectively; and a Lorentzian distribution of resonant transition energies is assumed (80). The measured macroscopic property $\chi^{(2)}$, is a sum of the molecular hyperpolarizability over all of the molecules at the interface, taking into account the orientation of the different molecular species. To obtain information on the orientation of the molecules, the observed Cartesian components of the macroscopic second-order susceptibility $\chi^{(2)}{}_{\rm IJK,\nu}$ must be derived from the corresponding spectroscopically active components of the molecular hyperpolarizability $\beta_{\rm lmn}$ through an Euler angle rotation of the molecular axis system into the laboratory axis system. Hirose et al (78, 79) derived a general expression for the transformation from a molecular fixed-axis system to a laboratory fixed-axis system as

$$\chi^{(2)}_{\rm IJK,\nu} = \sum_{\rm lmn} \mu_{\rm IJK:lmn} \cdot \beta_{\rm lmn,\nu}. \qquad 5.$$

The indices I, J, and K are replaced by the laboratory frame coordinates X, Y, and Z, respectively, observed in a specific experiment. The indices *l*, *m*, and *n* run through the molecular coordinates a, b, and c. The orientation of the molecular axis system in the laboratory frame is defined by the transformation tensor, $\mu_{\rm IJK:lmn}$ through the Euler angles (θ, ϕ, and χ). If the signs of $\beta_{\rm lmn,\nu}$ and $\chi^{(2)}{}_{\rm IJK,\nu}$ are known, the average orientation of the molecules can be constrained by analyzing how the sign of the transformation tensor changes with respect to the angles θ, ϕ, and χ. The signs of the $\chi^{(2)}{}_{\rm IJK,\nu}$ terms in Equation 5 are known through a comprehensive fit of the observed SF spectra to Equations 2 and 3, and the signs of the $\beta_{\rm lmn,\nu}$ components are known through ab initio calculations (81).

In many respects, the CCl_4/H_2O spectrum is a good test of the analysis, given the weakly interacting nature of the observed water molecules and hence the narrow bandwidths. For example, under I_{SSP} polarization, the SS and AS of monomeric H_2O would be expected to have opposite sign conventions (plus and minus, respectively), meaning that they are nearly 180° out of phase (57). Given that the OH dangling bond (plus sign convention) has a significant contribution perpendicular to the interface, if the water monomers are oriented with their dipoles in the same direction as the dangling bond, the SS(+) and AS(−) modes should interfere constructively and destructively, respectively, with the dangling bond mode. This is verified by fitting the data with the appropriate phase relationships using Voigt profiles (Figure 2*b*). Brown et al conclude from the fits and the derived sign of the phases that the SS and AS observed intensities represent water monomers at the interface that have a net orientation with their hydrogen atoms pointed into the CCl_4. The peak energies and widths determined from the fits agree well with Fourier transform IR data of water monomers in bulk water. Spectral fits place the AS and SS of these monomer and monomer-like waters with their hydrogen atoms oriented into the CCl_4 phase at 3616 ± 2 cm^{-1} and 3706 ± 2 cm^{-1}, respectively, compared with the Fourier transform IR-measured peaks at 3616 cm^{-1} and 3708 cm^{-1}. The experimental results are in agreement with

the molecular dynamics calculation of Chang & Dang for the CCl_4/H_2O interface (77).

EFFECT OF SURFACTANT ADSORPTION

Characterizing the interaction between water and a charged surfactant is important for understanding surfactant behavior in commercial soaps and detergents. However, it also is relevant to our understanding of many biological processes, including the folding of proteins where water interacts with charged groups on a hydrocarbon backbone. The series of studies described below focused on understanding how the hydrogen bonding of water is altered in the presence of increasing concentrations of simple charged alkyl surfactants. These studies were conducted at both the CCl_4/H_2O and air-water interfaces.

The hydrogen bonding of water is highly sensitive to the presence of charged surfactants, with changes occurring in the water spectrum at trace concentrations in the aqueous phase (LF Scatena & GL Richmond, manuscript in preparation). Figure 3 demonstrates this effect for the CCl_4/H_2O interface. When sodium dodecyl sulfate (SDS) is added in nanomolar concentrations to the aqueous phase, the trace SDS that adsorbs at the interface causes a dramatic change in the water spectrum that continues as the interfacial concentration increases to a monolayer, as seen by a comparison of Figure 2*a* with Figure 3*a*. As small amounts of SDS adsorb at the interface, the spectrum shows a strengthening in the hydrogen bonds between water molecules. The dangling OH bond essentially disappears as interfacial concentrations increase toward fractions of a monolayer. Further detailed studies of this effect at low concentrations in the nanomolar range will appear in a later publication. At higher concentrations, there is a multifold enhancement in the OH intensity, as shown by the difference in intensities displayed in Figure 3*b*.

The effect on the water spectrum of adding surfactants at aqueous-phase concentrations in the $>10^{-4}$ M range has been the focus of studies from this laboratory (82–84). In the absence of a charged surfactant or a mixture of anionic and cationic surfactants at the interface, this enhancement is not present. Figure 4 demonstrates this effect for SDS, dimethylammonium chloride (DAC), and a mixture of the two compounds at the air-water interface. The data were taken with *SSP* polarization that samples water dipoles oriented perpendicular to the interface. As shown, increased intensity is observed in the OH stretch region, which corresponds to strong hydrogen-bonding modes in the 3100–3500 cm^{-1} region of the water spectrum. For both interfaces, this intensity increases with added interfacial surfactant concentration, with a leveling off in the intensity that occurs well before monolayer formation (84). Figure 5 demonstrates this effect for a series of increasing concentrations of SDS at the CCl_4/H_2O interface. In these studies, the free OH mode was not studied owing to limited wavelength capabilities in the 3600 cm^{-1} region.

A series of detailed studies has been conducted to identify the factors that contribute to the enhanced VSF signal from water in the presence of charged surfactants

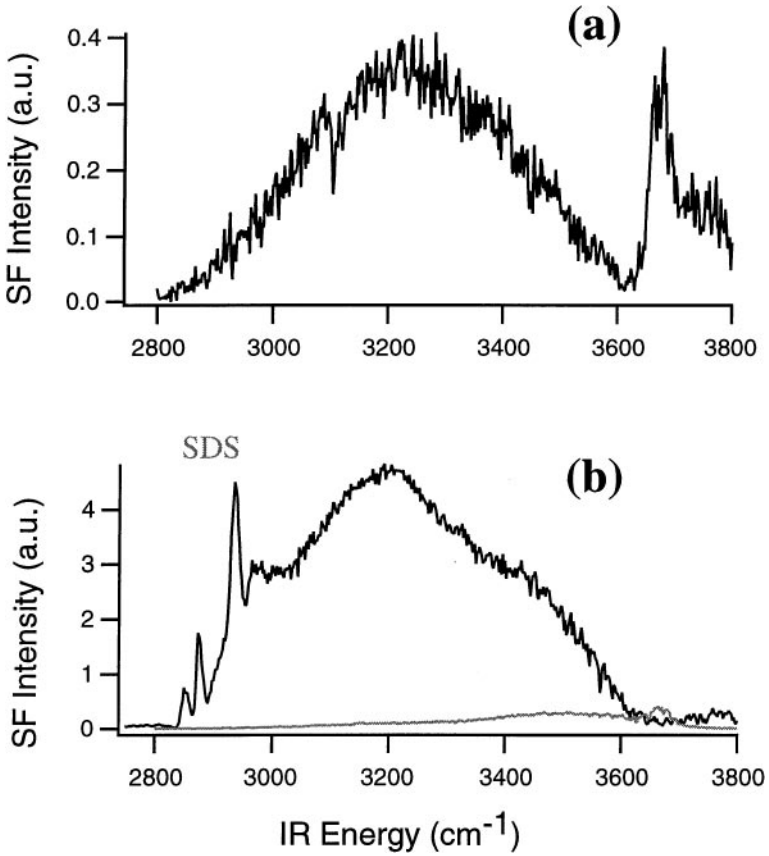

Figure 3 Effect of addition of sodium dodecyl sulfate (SDS) on the spectrum of water at the CCl_4/H_2O interface using *SSP* polarization. (*a*) Vibrational sum frequency (VSF) spectrum of the interface with 292-nM concentration of SDS in the aqueous phase; head group area $\gg 10^4$ A^2 molecule^{-1}. (*b*) VSF spectrum with 5 mM SDS in the aqueous phase. This corresponds to approximately a monolayer of SDS at the interface. The CH stretch modes are apparent near 2900 cm^{-1}. The gray line corresponds to the signal from the neat CCl_4/H_2O interface. From L. Scatena and G. L. Richmond, unpublished data.

(71, 84–86). Two factors have been considered. The simplest is the increased orientation of water molecules perpendicular to the interface that is caused by the large electrostatic field, E_0, created by the surfactant and its counterion. A significant surface charge exists at an interface where charged surfactant is adsorbed; this charge produces the large electrostatic field. An additional contribution to the *SF* polarization arises from a third-order polarization in Equation 6,

$$P_{\mathrm{sfg}} = \chi^{(2)} : E_{\mathrm{vis}} E_{\mathrm{ir}} + \chi^{(3)} : E_{\mathrm{vis}} E_{\mathrm{ir}} E_0, \qquad 6.$$

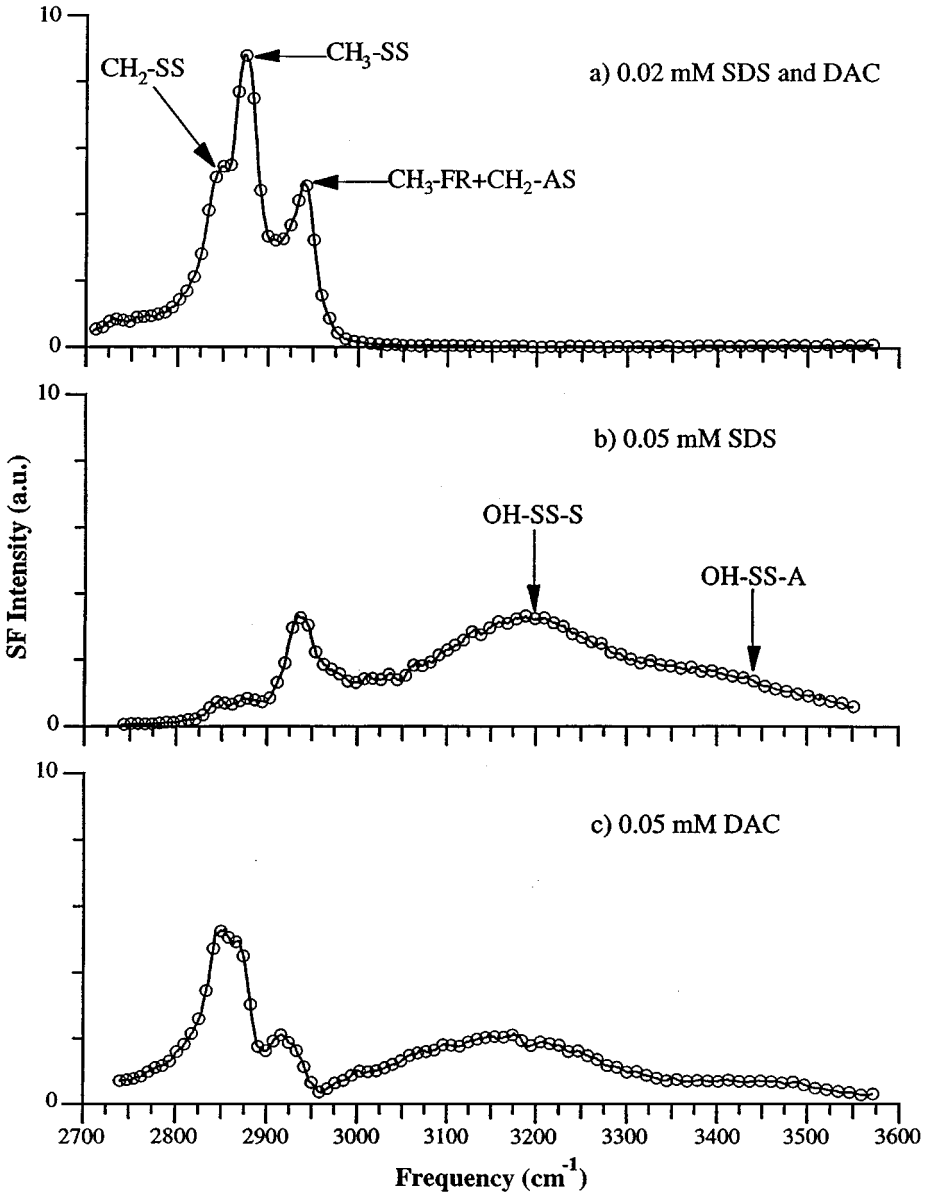

Figure 4 Vibrational sum frequency spectra under *SSP* polarization conditions from the air-water interface of an aqueous solution of (*a*) a mixture of 0.02 mM dimethylammonium chloride (DAC) and 0.02 mM sodium dodecyl sulfate (SDS), (*b*) 0.05 mM SDS, and (*c*) 0.05 mM DAC. Solid curves are a guide to the eye. Published with permission from Reference 89.

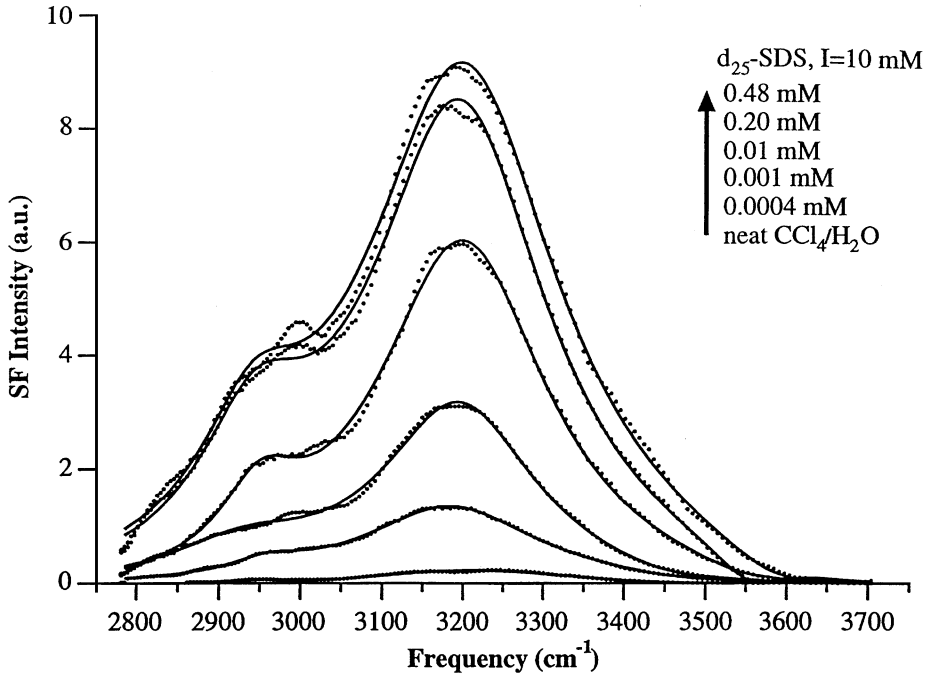

Figure 5 Vibrational sum frequency spectra from the CCl_4/SDS/H_2O interface under *SSP* polarization conditions for various bulk concentrations of sodium dodecyl sulfate (SDS) and an ionic strength of 10 mM. Solid curves are least squares fit to the data. Deuterated SDS (d_{25}) was used. Vibrational modes assigned include the methyl symmethic stretch (CH_3SS), methylene symmetric stretch (CH_2SS), methylene asymmetric stretch (CH_2AS) and Fermi resonance (FR). Published with permission from Reference 84.

which contains the electrostatic field dependence of the nonlinear polarization induced at the interface. In the absence of a large electrostatic field, the interfacial water molecules are randomly oriented after a few water layers and thus do not contribute to the nonlinear polarization. The presence of a large electrostatic field aligns the interfacial water molecules beyond the first few water layers and thus removes the centrosymmetry in this region, allowing more water molecules to contribute to the nonlinear polarization. The depth of the asymmetric region is on the order of the Debye length or 3 nm at an ionic strength of 10 mM, and 10 nm at an ionic strength of 1.0 mM. This depth corresponds to ~10–30 water layers, respectively (84). As a consequence, the second factor in the observed enhancement in the OH-stretching region is the increased number of water molecules that are sampled, owing to the contribution from the $\chi^{(3)}$ term in Equation 6.

To confirm this enhancement, studies comparing the VSF response with the interfacial potential have been conducted at a series of surfactant concentrations and ionic strengths (84). Assuming that $\chi^{(3)}$ is constant over the interfacial region,

the interfacial potential can be shown to have a linear relationship with P_{sfg}. Using the Gouy-Chapman model (87, 88), interfacial potential can be expressed as a function of surface charge density and ionic strength as

$$\Phi(0) = \frac{2kT}{ze}\sinh^{-1}\left(\sigma\sqrt{\frac{\pi}{2\varepsilon kTI}}\right), \qquad 7.$$

where σ is the surface charge density, z is the sign of the charged surfactant molecule, and I is the ionic strength of the bulk solution. The concentration and ionic strength studies confirm that a significant portion of the observed enhancement in the OH-stretching region is caused by the increased volume of water molecules, which gives rise to the VSF response (84). However, the lack of linearity between P_{sfg} and the surface potential for both interfaces suggests that orientation also contributes to the enhancement, that is, that there is alignment in the interfacial water molecules that accompanies the interfacial electrostatic field produced by the charged surfactant.

As in the neat water interfacial studies described above, interference between adjacent modes assists in determining the orientation of the water molecules at these charged interfaces. Analysis of the interference between the CH stretch modes and the water bands indicates that for cationic surfactants the water dipoles are oriented with their hydrogen atoms pointed toward the bulk aqueous solution. For anionic surfactants, water molecules are oriented with their oxygen atoms pointed toward the bulk aqueous solution (89).

STUDIES OF ENVIRONMENTALLY RELEVANT AQUEOUS-PHASE–AIR INTERFACES

The chemistry that occurs in the atmosphere involves both homogeneous and heterogeneous processes. Atmospherically important reactions have been studied extensively in the gas phase, but few published studies have examined in molecular detail the adsorption, molecular properties, and reactivity of atmospherically relevant molecules at water surfaces. Several studies dealing with organosulfur adsorbates on water surfaces have recently appeared, specifically studies of dimethyl sulfoxide (DMSO) and methane sulfonic acid (MSA) (56, 68, 90). Both molecules are present as trace constituents in the atmosphere and, although water soluble, have significant surface activities. DMSO has been proposed as a heterogeneous precursor to atmospheric condensed-phase MSA through an atmospheric cycle originating with dimethyl sulfide, a phytoplankton degradation product (91–93). Aerosol particles containing MSA are thought to contribute to the class of aerosols that effectively scatters radiation out of the atmosphere (92, 94). The molecular structure and orientation of DMSO have been examined in two studies, one of which looked at how the molecule changes as a function of surface concentration (90) and a second that examined the DMSO-water interaction at vapor-water interfaces. For neat DMSO studies, the methyl transition dipole moment is oriented

a maximum of 55° from the surface normal on average (90). Aqueous solutions of DMSO show that this molecule partitions to the surface. With decreasing DMSO concentration in an aqueous phase, observed VSF spectral shifts in the methyl-stretch mode have been attributed to increased electronic interactions between sulfur and the methyl groups of DMSO. Evidence is provided for clustering of DMSO molecules at the surface at higher interfacial concentrations. The second study of DMSO was conducted with improved spectral resolution and VSF detection to allow a more detailed analysis of the VSF spectrum of DMSO at the water surface, particularly interference between the methyl SS and AS modes, and the OH stretch modes of water in this region (68). With increased DMSO adsorption, a decrease in the intensity of the OH stretch mode of highly coordinated water molecules is observed. Allen et al attributed this effect to the strength of the hydrogen bonds that DMSO forms with water, which are stronger than those between water molecules and thus effectively disrupt the long-range order of the hydrogen-bonding network. MSA also partitions at the surface and has a preferred orientation in which the MSA methyl group points away from the liquid surface (56). The surrounding surface water structure is significantly affected by the adsorption of MSA, with small amounts of MSA found to enhance the intermolecular hydrogen bonding between interfacial water molecules. Studies with mixtures of water and sulfuric acid show that MSA is effectively displaced by sulfuric acid at an aqueous surface (56). Other VSF studies have examined the water structure in the presence of different acids, including sulfuric and nitric acid (65, 95–97). The VSF of surface water containing a series of salts has also been examined and shows how the surface is perturbed by the presence of these species in the bulk and surface phase (67).

SURFACTANT STUDIES AT LIQUID SURFACES

Interest in the adsorption of surfactants at liquid surfaces stems from the wide application of surfactants in commercial products. Although most surfactants are still used for conventional cleaning and hygiene purposes, they are also widely used as stabilizing foams and emulsions in food processing and in beverages, in the stabilization of particulate dispersions, and in the secondary recovery of oil from porous rock beds (98, 99). All of these uses depend on the amphiphilic character of the molecule—part nonpolar hydrophobic hydrocarbon and part polar hydrophilic moiety.

Monolayers of surfactants assembled at solid surfaces have been extensively studied during the last decade. What has been learned from these studies is that the assembly and ordering of these surfactant monolayers are affected by van der Waals interactions between the alkyl chains of adjacent surfactants. For liquid surfaces where the surfactants are not covalently bound to the surface and the interface is more dynamic, head group–head group and head group–solvent interactions have the potential to play a significant if not more important role than that played by

chain-chain interactions in the assembly process. In the presence of a solvent that can penetrate between the alkyl chains of the surfactants, such as for liquid-liquid interfaces, the picture is often even more complicated. This section describes the results of a number of studies of surfactant structure and conformation that were conducted at both the air-water and liquid-liquid interfaces. This summary is not intended to be comprehensive but merely provides an overview of the types of studies conducted thus far with VSFS. An example that demonstrates the difference in the assembly of surfactants at these two interfaces is highlighted.

VSF studies of surfactants have largely examined the CH stretch modes of the alkyl chains of various surfactants as a means of determining conformational ordering. Conformational ordering is qualitatively monitored by measuring the ratio of peak areas for the methyl SS and methylene SS modes in the VSF spectra (38). Under *SSP* polarization, chains that are relatively ordered and have few gauche defects should show little if any signal from the methylene CH stretch modes, owing to the symmetry of the molecule. In contrast, gauche defects owing to conformational disordering cause the VSF intensity of the methylene modes to increase as local symmetry constraints are relaxed. The terminal methyl group, which possesses both IR- and Raman-active vibrational modes, is by nature in a noncentrosymmetric environment and is further used in polarization experiments to determine the tilt angle of the hydrocarbon chain in these systems (100).

Surfactants at the Air-Water Interface

Some of the first VSF studies of surfactants measured at the air-water interface involved pentadecanoic acid (100). By monitoring the CH stretch region of the alkyl chains, it was found that, in the condensed phase, the alkyl chains extend and orient nearly normal to the surface. In the liquid expanded phase, the chains are highly disordered (100, 101). In a later related study, a carboxylic acid film of hexacosanaoic acid was studied at the air-water interface (102). The CH modes of the alkyl chains, the CO stretch in the head group, and the OH stretches of surface water have been monitored as a function of pH. The alkyl chains remained conformationally ordered at all pH values. At low pH values, at which the monolayer is neutral, the surface water is disordered by hydrogen bonding of water molecules with acid head groups. At high pH values, at which the head groups are ionized, the resulting surface fields lead to a more ordered hydrogen-bonding network.

Bell et al (103) have investigated the structure of monolayers of cationic surfactant, hexadecyltrimethylammonium *p*-tosylate, at the surface of water. They find that the *p*-tosylate ions are oriented with their methyl groups pointing away from the aqueous subphase and with the C_2 axis tilted an average of 30 to 40° from the surface normal. The vibrational spectrum of the cationic surfactant indicates that the number of gauche defects in the monolayer does not change dramatically when the counterion is changed from *p*-tosylate to bromide. However, the ends of the surfactant's hydrocarbon chains are tilted much farther from the surface normal in the presence of *p*-tosylate than in the presence of bromide. Alkyl cationic surfactant

(tetradecyl-trimethylammonium) with an aromatic anionic counterion (benzoate) has also been examined by Ward et al (104). Other studies of the effect of different halide counterions on monolayers of cationic surfactants at the air-water interface found no evidence for specific effects on the structure of the surfactant monolayers (105).

A series of soluble surfactants has also been examined and compared at the air-water interface by Bell et al (106). Bell et al find that, in general, the number of gauche conformations increases as the area per chain increases. Comparison of surfactants with the same chain length and area per molecule shows that the structure of the chain region of the monolayer is sensitive to the nature of the head group and not just to the packing density.

Monolayers of nonionic surfactants poly(ethylene glycol) monodecyl ethers ($C_{12}E_m$; $m = 2$–8) have been examined at the air-water interface (107). The results show an increase in conformational disorder with increasing area per molecule and an apparent decrease in the angle of tilt of the methyl group. The study also suggests that the value of m does not affect the structure of the monolayer for $m = 4$–8. In another study of uncharged surfactants, Zhang et al (108) have examined the adsorption of long-chain amphiphiles containing the nitrile (CN) head group. These air-water studies monitored the spectroscopy of the CN stretch modes and the CD stretch modes of the terminal CD_3 moiety on the alkyl chains of these Langmuir monolayers. The results indicate that the orientations of the head group and terminal methyl group vary in a markedly different manner with amphiphile surface density. For the CN head group, Zhang et al observe a sharp change in the orientation angle of that group, with surface density at the density corresponding to a phase transition from the gas-liquid coexistence region to the liquid region. This change is discussed in terms of the difference in solvating water environment during the phase transition. The orientation of the tail is quite sensitive to the monolayer density, with the tail continuously becoming more upright upon compression.

Mixed monolayers of SDS and dodecanol at the air-water interface have been studied by Casson & Bain (109). They find that when a trace of dodecanol is introduced into a millimolar solution of SDS, the monolayer is transformed from a loosely packed structure to a densely packed structure like that of a pure dodecanol monolayer. Temperature-dependent studies suggest that this mixed monolayer undergoes a phase transition at 16°C, with a decrease in packing and an increase in conformational disorder. This behavior is analogous to that observed in a pure dodecanol monolayer. From these results Casson & Bain conclude that previously reported phase transitions for SDS at the air-water interface are probably a result of the presence of trace amounts of dodecanol in the SDS. Later studies provide evidence for a liquid-gas phase transition in monolayers of dodecanol adsorbed at the air-water interface (110).

Stanners et al (111) have examined the adsorption at the air-water interface of a series of alcohols from C_1 to C_8 in the CH and OH stretch regions. They find that the alkyl chains point away from the liquid for all alcohols studied. For C_6–C_8, the spectra show the presence of *trans*-gauche defects in the alkyl chain. The shift of

spectra to lower frequency in the OH stretch region that was found for all alcohols indicates a well-ordered hydrogen-bonding network at the interface. Longer-chain alcohols have been pursued in other studies (112, 113).

Surfactants at Liquid-Liquid Interfaces

Surfactants studied at a liquid-liquid interface pose a challenge owing to the buried nature of the interface. Both the IR and visible beams must transmit through one of the solvents, but the number of solvents that are transparent in the spectral region of the surfactant vibrational modes is few. Even the weak IR absorbance caused by a thin layer of solvent can greatly diminish the incident IR beam. The most common organic solvent that has minimal absorption in the IR and is also insoluble in water is CCl_4. Therefore, all of the studies thus far of surfactants at liquid-liquid interfaces have been conducted at the CCl_4-water interface.

The first experiments in this area demonstrated the feasibility of using VSFS to measure the spectroscopy of charged alkyl surfactants at a liquid-liquid interface with a TIR geometry. D_2O has been used as the aqueous phase to minimize OH interference in these experiments. The studies demonstrate the ability to use TIR VSFS to measure interfacial concentrations of SDS below 0.01 monolayers. The studies have monitored the CH stretch modes of this surfactant and have shown that, whereas there is increased conformational ordering with interfacial concentration, the surfactants show significant gauche defects in the alkyl chains even at the highest concentrations. This result is attributed to interactions with the solvent that disrupt the van der Waals interactions between adjacent alkyl chains (38, 114). Polarization studies indicate that the terminal methyl group on the alkyl chain is oriented, on average, along the surface normal. Deuteration studies have been conducted to confirm the assignment of several CH vibrational modes. Later related studies examined a series of cationic and anionic surfactants of similar chain length, SDS, sodium dodecyl sulfonate (DDS), dodecyltrimethylammonium chloride (DTAC), and DAC, to understand how the different head groups alter the molecular conformation of the alkyl chains (70, 115). Figure 6 shows examples of the spectra of these molecules measured at the CCl_4/H_2O interface using *SSP* (see Figures 6*a*, *c*, *e*, *g*) and *SPS* (see Figures 6*b*, *d*, *f*, *h*) polarizations. The alkyl chains of the cationic surfactants possess the fewest gauche defects. Mixed cationic and anionic surfactants present at the interface lead to an increase in

Figure 6 Vibrational sum frequency spectra acquired with *P*-polarized IR and *S*-polarized visible light: (*a*) sodium dodecyl sulfate (SDS), (*c*) sodium dodecyl sulfonate (DDS), (*e*) dodecyltrimethylammonium chloride (DTAC), and (*g*) dodecylammonium chloride (DAC). Sum frequency (SF) spectra were acquired with *S*-polarized IR and *P*-polarized visible light: (*b*) SDS, (*d*) DDS, (*f*) DTAC, and (*g*) DAC. Spectra were obtained at the CCl_4/D_2O interface with a bulk aqueous-phase concentration of 5.0 mM for all of the surfactants studied. The generated SF was *S*-polarized in all cases. The solid curves represent a fit to the spectra using a combination of Gaussian and Lorentzian functions for each peak. Reproduced with permission from Reference 115.

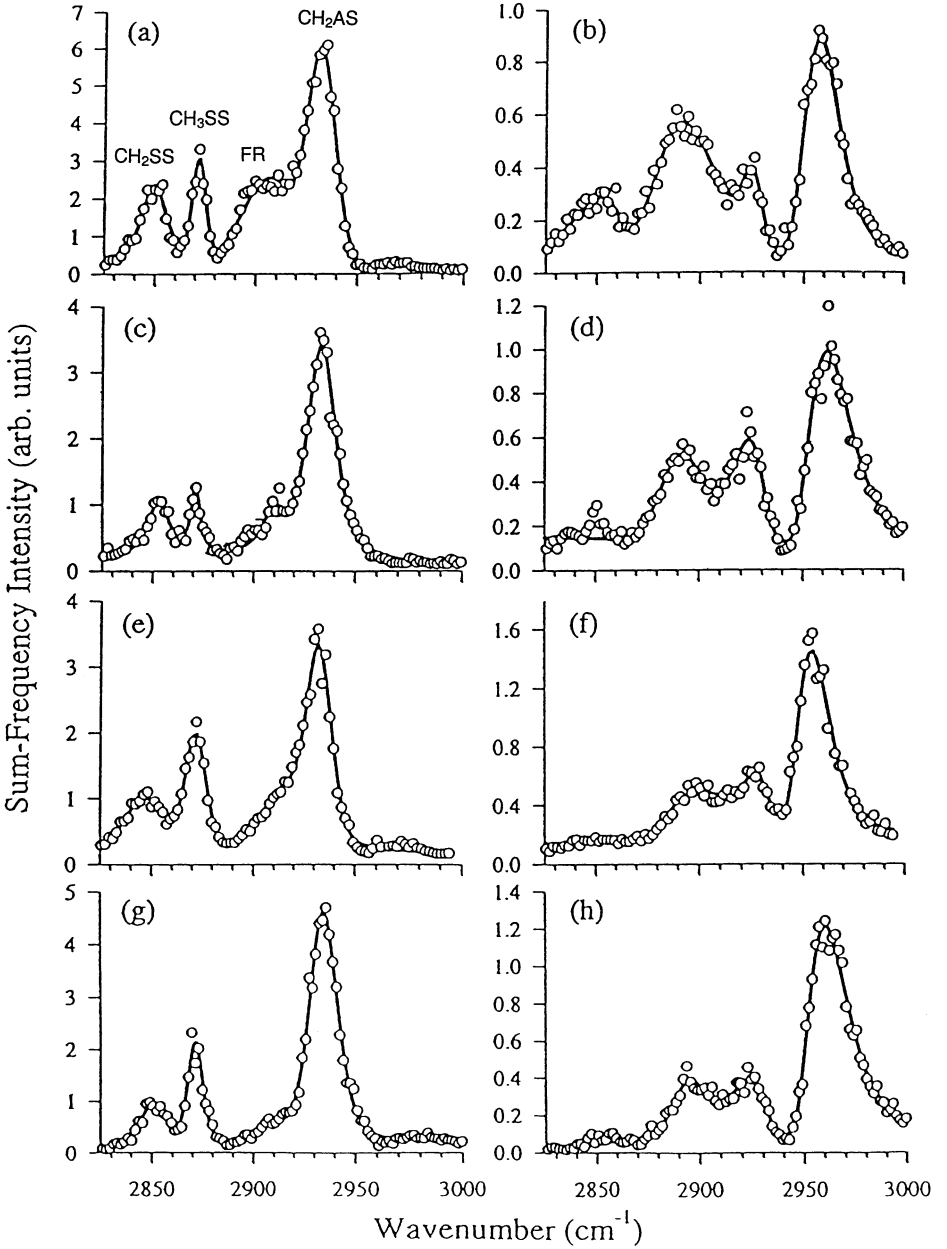
(a)
CH2AS
CH3SS
CH2SS
FR
(b)
(c)
(d)
(e)
(f)
(g)
(h)
Sum-Frequency Intensity (arb. units)
Wavenumber (cm-1)
2850
2900
2950
3000

ordering of the chains, which is attributed to a reduction in head group repulsion at the interface. Studies of sulfonate-containing surfactants of different chain lengths find that the degree of disorder varies greatly with chain length for the surfactants at the CCl_4/D_2O interface (116). The shortest alkyl chain, C_6, displays the fewest gauche defects, and the longest chains, C_{11} and C_{12}, show the most disorder. No preference in ordering like that often found for monolayers on solid surfaces is observed between even and odd chain surfactants.

Comparative Studies at Both Liquid-Liquid and Liquid-Air Interfaces

One of the more interesting studies that demonstrates the differences and similarities in how surfactants adsorb, orient, and order themselves at a liquid-liquid versus an air-water interface has been conducted with alkyl and aryl sulfonate surfactants by Watry & Richmond (117). Linear alkane sulfonate surfactants and linear alkylbenzenesulfonates (LABS) make up a large fraction of the surfactants used in commercial detergents and cleansers, with LABS being one of the most widely used. The two surfactants studied by Watry & Richmond were DDS and sodium dodecylbenzenesulfonate (DBS). Figure 7 shows a spectrum of DBS measured at the CCl_4/H_2O interface (Figure 7*a*) and the air-water interface (Figure 7*b*), both with *SSP* polarizations. Because the two experiments were conducted with different laser systems, peak positions can be compared but not absolute intensities. The CH stretch modes of the alkyl chains are clearly observed, as are the expected modes ν_{7b} and ν_2 of the aromatic ring. Polarization studies have been used to monitor how the orientation of the benzene ring in DBS changes with interfacial concentration. Figure 8 shows a plot of the ν_2 intensity as a function of surface concentration for DBS at the air-water interface (Figure 8*a*) and the CCl_4/D_2O interface (Figure 8*b*). The liquid-liquid interface shows a monotonic increase in intensity with surface concentration. The benzene rings orient perpendicularly to the interface, and this orientation is not affected by changes in interfacial concentration even at surface concentrations up to a monolayer. This is in stark contrast to the effects observed at the air-water interface (Figure 8*a*). A sharp increase in intensity is observed as monolayer coverage is approached, which suggests that the increased interaction between the benzene rings as the surface concentration increases causes a change of orientation from a more planar to a perpendicular orientation relative to the surface plane. The different behaviors of the aryl group at the two interfaces are attributed to different interfacial potentials and the presence of polarizable CCl_4, which causes the benzene rings to continue their initial orientation at the liquid-liquid interface but to change in orientation at the air-water interface once crowding and increased benzene-benzene interactions occur.

The alkyl chain conformation for these two molecules at the different interfaces has also been compared. For DDS, the alkyl chains increase in conformational ordering as the interfacial concentration is increased at both interfaces. For DBS, a high degree of gauche defects is apparent in the chains at all concentrations at both

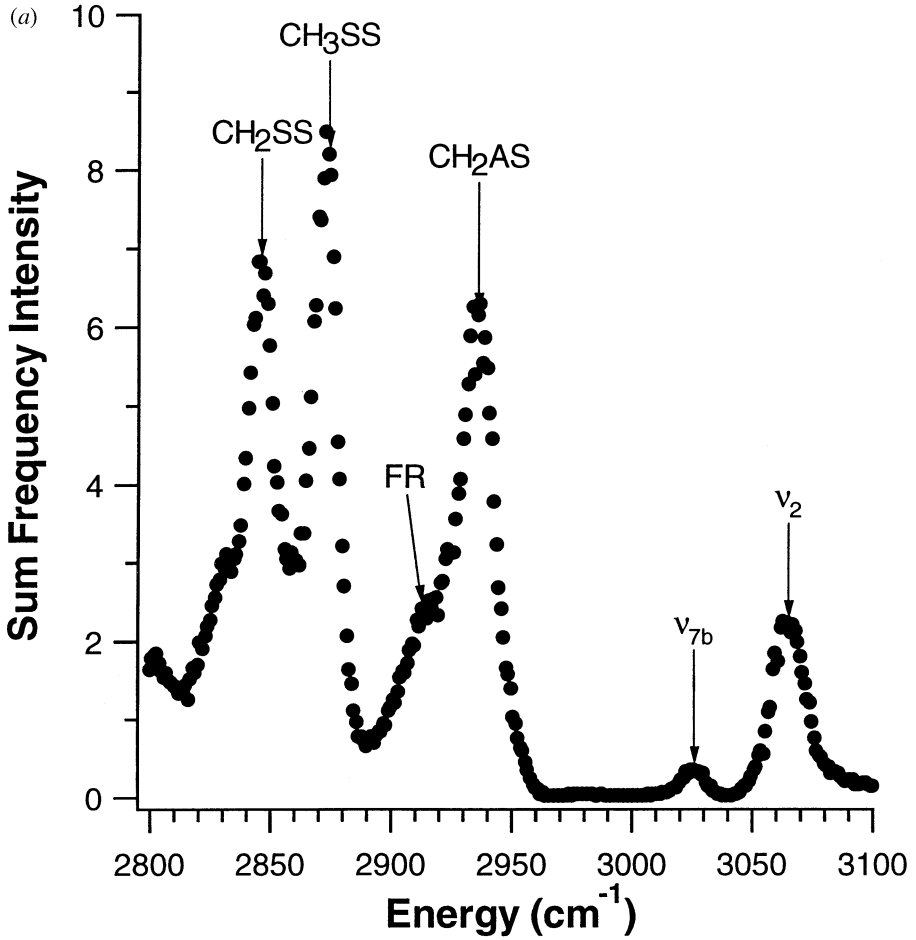

Figure 7 Vibrational sum frequency spectrumof (*a*) sodium dodecylbenzenesulfonate at the CCl_4/D_2O interface under conditions of 0.1 M NaCl, *SSP* polarization, and 1-ns laser pulses, and (*b*) sodium dodecylbenzenesulfonate at the air-D_2O interface, under conditions of 0.1 M NaCl, *SSP* polarization, and 2-ps laser pulses. Solid curves are fits to the data assuming a Voigt functional form for the peaks. Reproduced with permission from Reference 117.

interfaces. At the air-water interface, the benzene reorientation of DBS appears to have minimal effect on alkyl chain ordering. A key to understanding these differences comes from measurements of the limiting surface area per molecule. These studies measure nearly identical surface head group areas for DDS and DBS at monolayer coverages ($\sim$60 A^2 $molecule^{-1}$) even though the geometric head group of DBS is much larger than DDS. This suggests that DBS surfactants exist in a staggered head group geometry, a picture that is consistent with the disruption

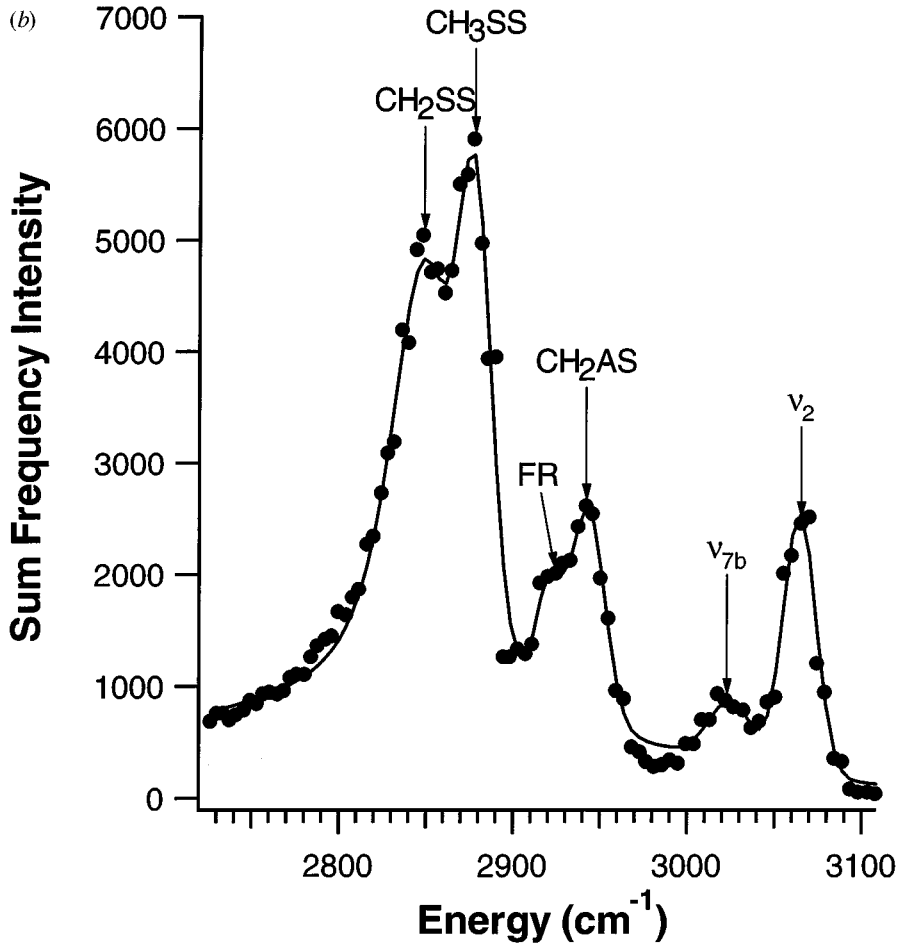

Figure 7 (*Continued*)

by the benzene rings of chain-chain interactions for the first few methylene groups adjacent to the benzene ring for DBS. There is no evidence that increased surface concentration and subsequent packing of alkyl chains can overcome this disruption.

BIOLOGICALLY RELEVANT SYSTEMS

Phospholipid Assembly

Phosphatidylcholines (PCs) are amphiphilic molecules possessing two long acyl chains connected to a zwitterionic head group by means of a three-carbon glycero backbone. These phospholipids are a major component of most cell membranes

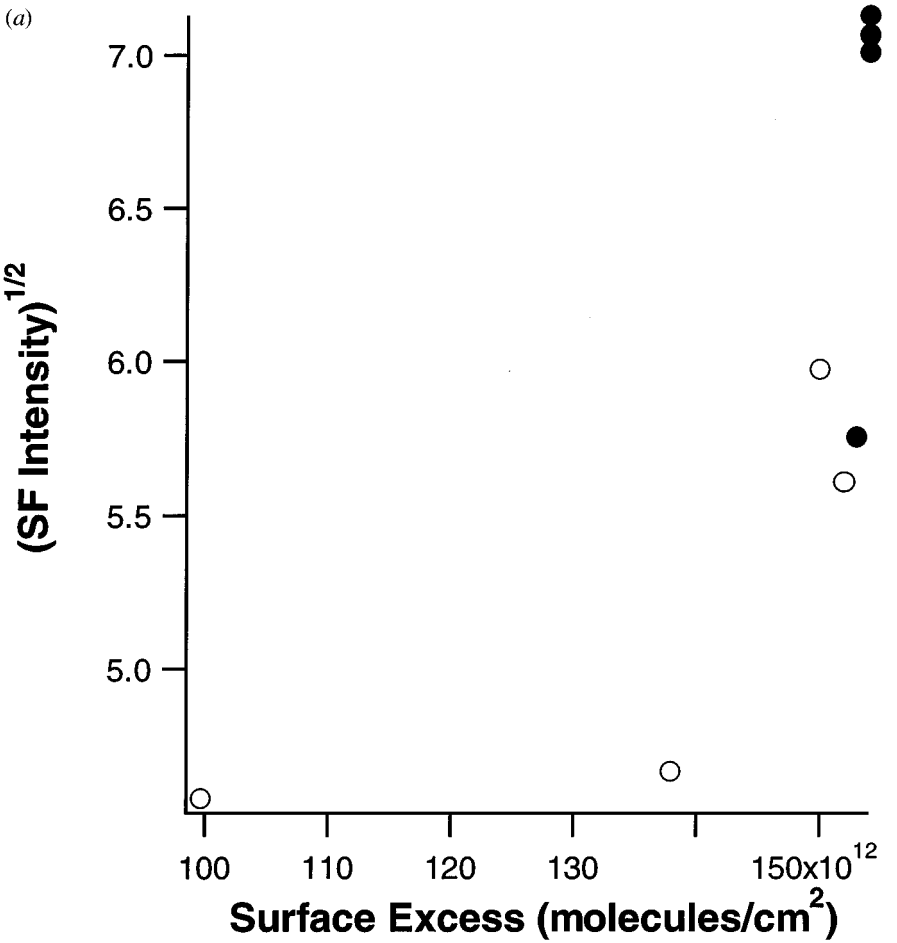

Figure 8 Square root of sum frequency intensity of the mode ν_2 as a function of surface concentration for (*a*) sodium dodecylbenzenesulfonate (DBS) at the air-water interface and (*b*) DBS at the CCl_4-water interface with 0.1 M NaCl. The line is a fit to the data. Solid circles indicate data points that correspond to concentrations at which the surfactant interfacial concentration is near a monolayer of coverage. Reproduced with permission from Reference 117.

and, consequently, have been the subject of intense scientific scrutiny over the past three decades. Cell membranes generally consist of a lipid bilayer structure, and PC monolayers have served as simple model membranes (118). VSFS studies of PC monolayers adsorbed at the CCl_4/D_2O interface and the air-water interface have been conducted to ascertain how the molecular structure of the monolayer depends on such variables as acyl chain length, surface concentration, temperature, and, by inference, the degree of chain solvation by the organic solvent (119). Some examples of these studies are given below.

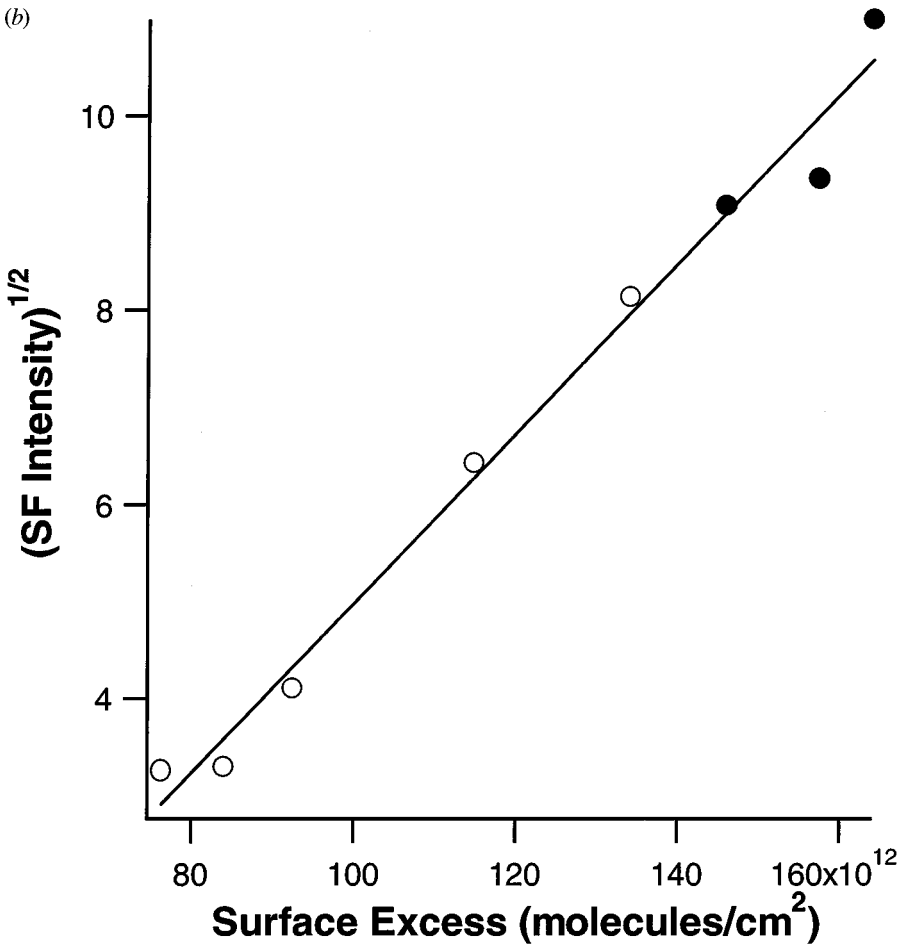

Figure 8 (*Continued*)

The first measurements of the vibrational spectroscopy of PCs at a liquid surface have been conducted with dialkylphosphocholines (Figure 9) (120). The four PCs examined included dilauroyl-PC (DLPC), dimyristoyl-PC (DMPC), dipalmitoyl-PC (DPPC) and distearoyl-PC (DSPC), with acyl chain units of C_{12}, C_{14}, C_{16}, and C_{18}, respectively. The CH stretch modes were used to determine conformational ordering of the chains in a manner similar to the surfactant studies described above. Figure 10 shows the spectra of the four PCs examined at the CCl_4/D_2O interface under *SSP* polarization. Conformational ordering of the chains has been determined by the ratio of areas under the d^+ (methylene symmetric stretch mode) and r^+ (methyl symmetric stretch mode). In the first set of studies of these PCs at the liquid-liquid interface it was found through temperature-controlled experiments that the lipid bilayer gel to liquid crystalline phase transition temperature plays

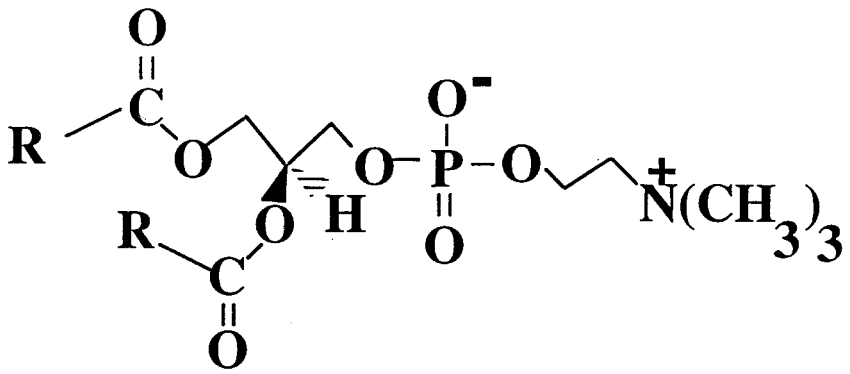

Figure 9 Molecular structure of dialkyl phosphocholines used in this study. $R = C_{n-1}H_2CH_3$ where $N = 12$ is dilauroyl-phosphocholine, $N = 14$ is dimyristoyl-phosphocholine, $N = 16$ is dipalmitoyl-phosphocholine, and $N = 18$ is distearoyl-phosphocholine.

a pivotal role in determining the interfacial coverage and subsequent alkyl chain structure. This and other aspects of PC adsorption have been studied in further detail by Walker et al (73). In these liquid-liquid studies, polarization experiments showed that the acyl chains do not exhibit long-range order. Acyl chains within a tightly packed monolayer are found to stand up with their methyl C_3 axes aligned perpendicular to the interface. Temperature studies of the monolayer order suggest that a barrier exists to organic solvent penetration of the acyl chain network of a tightly packed, adsorbed monolayer. At the liquid-liquid interface, it is found that shorter-chain PC species form monolayers that are more ordered than those of longer-chain species, although the dependence of monolayer order on acyl chain length is small. When identical studies are conducted at the air-water interface, the opposite trend is observed. That is, the longer-chain PCs form monolayers that are dramatically more ordered than those of their shorter-chain counterparts. This difference can be seen in Figure 11, where ratios of r^+/d^+ for the PCs at the different interfaces are compared. This disparity provides evidence for acyl chain solvation by the organic CCl_4 solvent.

A study by Smiley & Richmond (121) has examined alkyl chain ordering of asymmetric PCs adsorbed at the CCl_4/D_2O interface. The large majority of biological phospholipids contain two dissimilar hydrocarbon chains per molecule. The two chains may differ in length and degree of unsaturation in such a way that a highly complex mixture of phospholipid structures is present in a particular bilayer membrane, allowing other structural elements to be accommodated without disruption

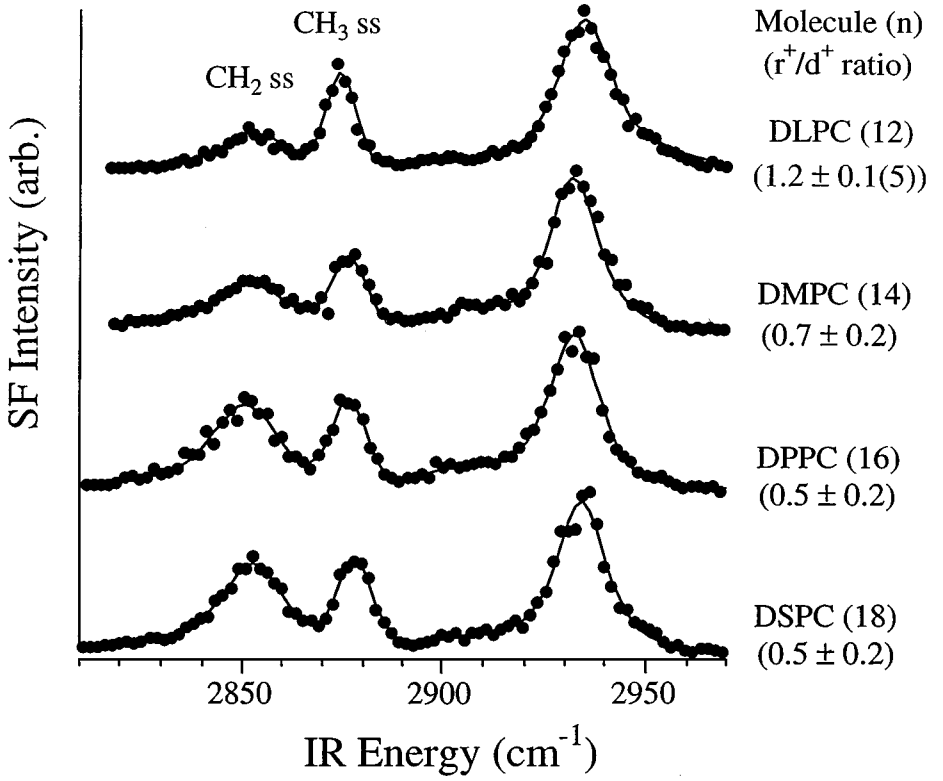

Figure 10 Vibrational sum frequency spectra of tightly packed monolayers composed of dilauroyl-phosphocholine (DLPC), dimyristoyl-phosphocholine (DMPC), dipalmitoyl-phosphatidylcholine (DPPC), and distearoyl-phosphatidylcholine (DSPC) at the water-CCl_4 interface. Ratios of the methylene SS intensity/methy SS intensity (r^+/d^+) appear underneath the PC acronyms. Spectral features were fit to Voigt profiles. Reproduced with permission from Reference 73.

of bilayer integrity (122). Smiley & Richmond have used a somewhat different preparation procedure than that used by Walker et al (73), owing to the insolubility of several of the PCs in water. These studies of a series of saturated symmetric and asymmetric chain PCs find that both symmetric PCs with 16 or fewer carbons per acyl chain and highly asymmetric PCs produce relatively disordered films at the liquid-liquid interfaces. The longest PCs studied, C_{18}/C_{18}, C_{18}/C_{16}, and C_{16}/C_{18}, form well-ordered monolayers at room temperatures. The highly disordered nature of the chains for the highly asymmetric PCs is consistent with a picture of reduced chain-chain interactions among mismatched portions of the longer chains. The greater disorder seen in the shorter-chain PCs, irrespective of chain mismatch, is attributed to reduced chain-chain interactions over a smaller chain length. This study has been further expanded to longer-chain PCs, up to C_{22} (123). The results show a strong increase in relative ordering for the longer-chain PCs, including

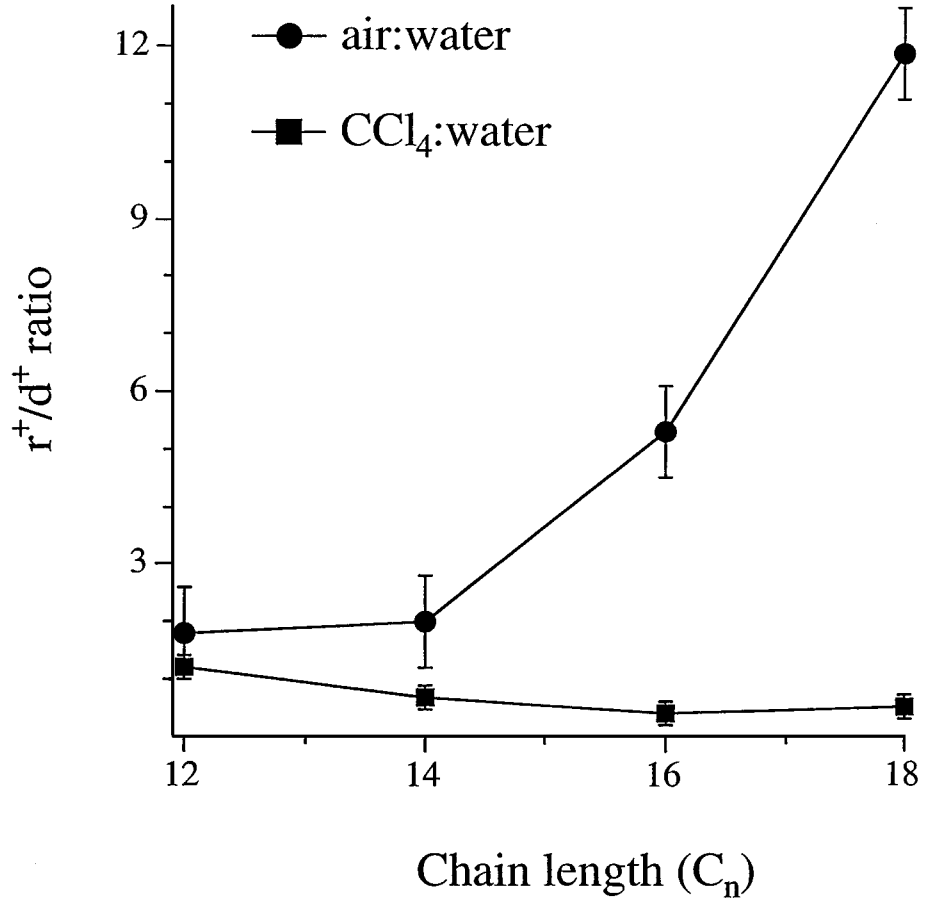

Figure 11 A comparison of the r^+/d^+ ratios for the different phosphatidylcholine monolayers at the air-water and CCl_4-water interfaces. Error bars reflect the uncertainty limits. Reproduced with permission from Reference 73.

those with an odd number of carbons per chain. The chain ordering of selected mixtures of adsorbed PCs is seen to be composition dependent, indicative of natural structural variances present in the large variety of functional biological membrane assemblies suited to a multitude of modes.

CONCLUSIONS

Obtaining a molecular level picture of liquid surfaces is a challenging area of surface science. From an experimental perspective, it is an exciting time to be delving into issues of this nature because of the emergence of many new experimental techniques that measure properties in the molecular domain. VSFS will clearly

play an important role in this field as has already been demonstrated over the past decade. This summary has provided an overview of many of the studies of liquid surfaces by VSFS that have been conducted since the first results were reported in the mid-1980s. The examples described include measurements of the molecular interactions between water molecules at the vapor-water and organic-matter–water interfaces, the effect of adsorbed species on water structure and hydrogen bonding, and studies of the conformation and assembly of surfactants, macromolecules, biomolecules, and atmospherically relevant molecules at these interfaces.

There are numerous opportunities and challenges for this technique in the future. Studies are beginning to emerge that go beyond the traditionally probed 3-μm region to longer wavelengths at which a variety of additional modes can be measured. Extension to these longer-wavelength regions will require continued development of IR generation methods and pulsed lasers. As other modes become spectroscopically accessible, challenges will arise in spectral interpretation owing to the coherent nature of the VSF response, similar to the challenges demonstrated in this review for water spectra. Close coupling of the knowledge base derived from IR and Raman molecular spectroscopy with nonlinear optical principles will be important in interpretation of the spectral data to derive meaningful and rigorous interpretation of the observed spectral response. VSF studies of simple systems will be very valuable as the field moves toward understanding of the structure of more complex biological and polymeric systems. Time-resolved measurements that take advantage of the short pulsed nature of the lasers used in VSFS offer additional exciting opportunities.

ACKNOWLEDGMENTS

The author gratefully acknowledges the support of the National Science Foundation (CHE-9725751), the Office of Naval Research, and the Department of Energy's Office of Basic Energy Sciences for various studies described in this review that originated from this laboratory.

LITERATURE CITED

1. Stillinger FH. 1980. *Science* 209:451
2. Stillinger FH. 1973. *J. Solut. Chem.* 2:141–58
3. Tanford C. 1973. *The Hydrophobic Effect: Formation of Micelles and Biological Membranes*. New York: Wiley-Intersci.
4. Wilson MA, Pohorille A, Pratt LR. 1987. *J. Phys. Chem.* 91:4873–78
5. Hummer G, Garde S, García AE, Paulaitis ME, Pratt LR. 1988. *J. Phys. Chem. B* 102:10469–82
6. Lum K, Chandler D, Weeks JD. 1999. *J. Phys. Chem. B* 103:4570–77
7. Sokhan VP, Tildesley DJ. 1997. *Mol. Phys.* 92:625–40
8. Taylor RS, Dang LX, Garrett BC. 1996. *J. Phys. Chem.* 100:11720–25

9. Stillinger FH, Ben-Naim A. 1967. *J. Chem. Phys.* 47:4431–37
10. Townsend RM, Rice SA. 1991. *J. Chem. Phys.* 94:2207–18
11. Weeks JD. 1997. *J. Chem. Phys.* 67:3106–21
12. Croxton CA. 1986. *Fluid Interfacial Phenomena*. New York: Wiley & Sons
13. Benjamin I. 1992. *J. Chem. Phys.* 97:1432–45
14. Schweighofer K, Benjamin I. 2000. *J. Chem. Phys.* 112:1474–82
15. Schweighofer KJ, Essmann U, Berkowitz M. 1997. *J. Phys. Chem. B* 101:3793–99
16. Gao J, Jorgensen WL. 1988. *J. Phys. Chem.* 92:5813–22
17. Carpenter IL, Hehre WJ. 1990. *J. Phys. Chem.* 94:531–36
18. Feller SE, Zhang Y, Pastor RW. 1995. *J. Chem. Phys.* 103:10267–76
19. vanBuuren AR, Marrink S-J, Berendsen HJC. 1993. *J. Phys. Chem.* 97:9206–12
20. Napari I, Laaksonen A, Talanquer V, Oxtoby DW. 1999. *J. Chem. Phys.* 110:5906–12
21. Linse P. 1987. *J. Chem. Phys.* 86:4177–87
22. Du Q, Freysz E, Shen YR. 1994. *Phys. Rev. Lett.* 72:238–41
23. Ren Y, Meuse CW, Hsu SL, Stidham HD. 1994. *J. Phys. Chem.* 98:8424–30
24. Willard DM, Riter RE, Levinger NE. 1998. *J. Am. Chem. Soc.* 120:4151–68
25. Chamberlain J, Pemberton JE. 1997. *Langmuir* 13:3074–79
26. Dluhy RA. 1986. *J. Phys. Chem.* 90:1373–79
27. Buontempo JT, Rice SA. 1993. *J. Chem. Phys.* 98:5835–46
28. Wolfrum K, Graener H, Laubereau A. 1993. *Chem. Phys. Lett.* 214:41–46
29. Bell GR, Bain CD, Ward RN. 1996. *J. Chem. Soc. Faraday Trans.* 92:515–23
30. Knobler CM. 1990. *Advances in Chemical Physics*. New York: Wiley & Sons
31. Fiehrer KM, Nathanson GM. 1997. *J. Am. Chem. Soc.* 119:251–52
32. Brezesinski G, Thoma M, Struth B, Mohwald H. 1996. *J. Phys. Chem.* 100:3126–30
33. Lu JR, Li ZX, Thomas RK, Penfold J. 1996. *J. Chem. Soc. Faraday Trans.* 92:403–8
34. Weinbach SP, Kjaer K, Bouwman W, Als-Nielsen J, Leiserowitz L. 1996. *J. Phys. Chem.* 100:8356–62
35. Israelachvili JN. 1996. *Intermolecular and Surface Forces*. New York: Academic
36. Eisenthal KB. 1996. *Chem. Rev.* 96:1343–60
37. Wirth MJ, Burbage JD. 1992. *J. Phys. Chem.* 96:9022–25
38. Conboy JC, Messmer MC, Richmond GL. 1996. *J. Phys. Chem.* 100:7617–22
39. Shen YR. 1989. *Nature* 337:519–25
40. Bloembergen N. 1966. *Opt. Acta* 13:311–22
41. Bloembergen N, Simmon HJ, Lee CH. 1969. *Phys. Rev.* 181:1261–71
42. Gragson DE, McCarty BM, Richmond GL, Alavi DS. 1996. *J. Opt. Soc. B* 13:2075–83
43. Tadjeddine A, Peremans A, Guyot-Sionnest P. 1995. *Surf. Sci.* 335:210–20
44. Bain CD. 1995. *J. Chem. Soc. Faraday Trans.* 91:1281–96
45. Gragson DE, Alavi DS, Richmond GL. 1995. *Opt. Lett.* 20:1991–93
46. McGuire JA, Beck W, Wei X, Shen YR. 1999. *Opt. Lett.* 24:1877–80
47. van der Ham EWM, Vrehen QHR, Eliel ER. 1996. *Opt. Lett.* 21:1448–50
48. Richter LJ, Petralli-Mallo TP, Stephenson JC. 1998. *Opt. Lett.* 23:1594–97
49. Scherer JR. 1978. In *Advances in Infrared and Raman Spectroscopy*, Vol. 5, ed. RJH Clark, RE Hester, pp. 149–216. Philadelphia: Heyden
50. Lippincott ER, Finch JN, Schroeder R. 1959. In *Hydrogen Bonding*. New York: Pergamon
51. Schuster P, Zundel G, Sandorfy C. 1976. *The Hydrogen Bond. Recent Developments in Theory and Experiment*. Amsterdam: North Holland
52. Eisenberg D, Kauzmann W. 1969. *The*

Structure and Properties of Water. New York: Oxford Univ. Press
53. Franks F. 1972. *Water: A Comprehensive Treatise*. New York: Plenum
54. Pimental GC, McClellan AL. 1960. *The Hydrogen Bond*. San Francisco: Freeman
55. Du Q, Superfine R, Freysz E, Shen YR. 1993. *Phys. Rev. Lett.* 70:2313–16
56. Allen HC, Raymond EA, Richmond GL. 2001. *J. Phys. Chem.* In press
57. Brown MG, Raymond EA, Allen HC, Scatena LF, Richmond GL. 2000. *J. Phys. Chem.* 104:10220–26
58. Goss LM, Sharpe SW, Blake TA, Vaida V, Brault JW. 1999. *J. Phys. Chem.* 103:8620–24
59. Falk M, Giguere PA. 1957. *Can. J. Chem.* 35:1195–204
60. Zundel G. 1976. In *The Hydrogen Bond*, Vol. II, *Structure and Spectroscopy*, Chap. 15, ed. P Schuster, G Zundel, C Sandorfy, pp. 687–766. New York: North-Holland
61. Walrafen GE, Yang WH, Chu YC. 1997. *ACS Symp. Ser.* 676:287–308
62. Hare DE, Sorenson CM. 1990. *J. Chem. Phys.* 84:25–33
63. Buch V, Devlin JP. 1999. *J. Phys. Chem.* 110:3437–43
64. Whalley E, Klug DD. 1986. *J. Chem. Phys.* 84:78–80
65. Schnitzer C, Baldelli S, Shultz MJ. 1999. *Chem. Phys. Lett.* 313:416–20
66. Simonelli DM, Baldelli S, Shultz MJ. 1998. *Chem. Phys. Lett.* 298:400–404
67. Schnitzer C, Baldelli S, Shultz MJ. 2000. *J. Phys. Chem. B* 104:585–89
68. Allen HC, Raymond EA, Richmond GL. 2000. *Curr. Opin. Colloids Surf.* 5:74–80
69. Du Q, Freysz E, Shen YR. 1994. *Science* 264:826–28
70. Conboy JC, Messmer MC, Walker R, Richmond GL. 1997. *Prog. Colloids Polym. Sci.* 103:10–20
71. Gragson DE, Richmond GL. 1997. *J. Chem. Phys.* 107:9687–90
72. Richmond GL. 1997. *Anal. Chem. News Views* 69:A536–43
73. Walker RA, Gruetzmacher JA, Richmond GL. 1998. *J. Am. Chem. Soc.* 120:6991–7003
74. Walker RA, Smiley BE, Richmond GL. 1999. *Spectrscopy* 14:18–22
75. Gragson DE, Richmond GL. 1997. *Langmuir* 13:4804–6
76. Ahlström P, Wallqvist A, Engström S, Jonsson B. 1989. *Mol. Phys.* 68:563–68
77. Chang T-M, Dang LX. 1996. *J. Chem. Phys.* 104:6772–83
78. Hirose C, Akamatsu N, Domen K. 1992. *Appl. Spectrosc.* 46:1051–72
79. Hirose C, Akamatus N, Domen K. 1992. *J. Chem. Phys.* 96:997–1004
80. Shen YR. 1984. *The Principles of Nonlinear Optics*. New York: Wiley & Sons
81. Fredkin DR, Komornicki A, White SR, Wilson KR. 1983. *J. Chem. Phys.* 78:7077–92
82. Walker RA, Richmond GL. 1999. *Colloids Surf. A* 154:175–80
83. Gragson DE, McCarty BM, Richmond GL. 1997. *J. Am. Chem. Soc.* 119:6144–52
84. Gragson DE, Richmond GL. 1998. *J. Am. Chem. Soc.* 120:366–75
85. Gragson DE, Richmond GL. 1998. *J. Phys. Chem. B* 102:569–76
86. Gragson DE, McCarty BM, Richmond GL. 1996. *J. Phys. Chem.* 100:14272–75
87. Zhao X, Ong S, Eisenthal KB. 1993. *Chem. Phys. Lett.* 202:513–20
88. Chattoraj DK, Birdi KS. 1984. *Adsorption and the Gibbs Surface Excess*. New York: Plenum
89. Gragson DE, Richmond GL. 1998. *J. Phys. Chem.* 102:3847–61
90. Allen HC, Gragson DE, Richmond GL. 1999. *J. Phys. Chem.* 103:660–66
91. Barone SB, Turnipseed AA, Ravishankara AR. 1995. *Faraday Discuss.* 100:39–54
92. Davis D, Chen G, Kasibhatla P, Jefferson A, Tanner D, et al. 1998. *J. Geophys. Res.* 103:1657–78
93. Jefferson A, Tanner DJ, Eisels FL, Davis DD, Chen G, et al. 1998. *J. Geophys. Res.* 103:1647–56

94. Charlson RJ, Lovelock JE, Andrae MO, Warren SG. 1987. *Nature* 326:655–61
95. Raduge C, Pflumio V, Shen YR. 1997. *Chem. Phys. Lett.* 274:140–44
96. Baldelli S, Schnitzer C, Shultz MJ, Campbell DJ. 1997. *J. Phys. Chem. B* 49:10435–41
97. Baldelli S, Schnitzer C, Shultz MJ, Campbell DJ. 1998. *Chem. Phys. Lett.* 287:143–47
98. Morse PM. 1999. *Chem. Eng. News* 35–48
99. Porter MR. 1994. *Handbook of Surfactants*. 2nd ed. Glasgow, UK: Chapman & Hall.
100. Guyot-Sionnest P, Hunt JH, Shen YR. 1987. *Phys. Rev. Lett.* 59:1597–600
101. Hunt JH, Guyot-Sionnest P, Shen YR. 1987. *Chem. Phys. Lett.* 133:189–92
102. Miranda PB, Du Q, Shen YR. 1998. *Chem. Phys. Lett.* 286:1–8
103. Bell GR, Li ZX, Bain CD, Fischer P, Duffy DC. 1998. *J. Phys. Chem. B* 102:9461–72
104. Ward RN, Duffy DC, Bell GR, Bain CD. 1996. *Mol. Phys.*. 88:269–80
105. Knock MM, Bain CD. 1999. *Langmuir* 16:2857–65
106. Bell GR, Bain CD, Ward RN. 1996. *J. Chem. Soc. Faraday Trans.* 92:515–23
107. Goates SR, Schofield DA, Bain CD. 1999. *Langmuir* 15:1400–9
108. Zhang D, Gutow J, Eisenthal KB. 1994. *J. Phys. Chem.* 98:13729–34
109. Casson BD, Bain CD. 1998. *J. Phys. Chem. B* 102:7434–41
110. Casson BD, Bain CD. 1999. *J. Am. Chem. Soc.* 121:2615–16
111. Stanners CD, Du Q, Chin RP, Cremer P, Somorjai GA, Shen YR. 1995. *Chem. Phys. Lett.* 232:407–13
112. Wolfrum K, Laubereau A. 1994. *Chem. Phys. Lett.* 228:83–88
113. Braun R, Casson BD, Bain CD. 1995. *Chem. Phys. Lett.* 245:326–34
114. Messmer M, Conboy JC, Richmond GL. 1995. *J. Am. Chem. Soc.* 117:8039–40
115. Conboy JC, Messmer MC, Richmond GL. 1997. *J. Phys. Chem.* 101:6724–33
116. Conboy JC, Messmer MC, Richmond GL. 1998. *Langmuir* 14:6722–27
117. Watry M, Richmond GL. 2000. *J. Am. Chem. Soc.* 122:875–83
118. Gershfeld NL. 1976. *Annu. Rev. Phys. Chem.* 27:349–60
119. Smiley BE, Walker RA, Gragson DE, Hannon TE, Richmond GL. 1998. *Proc. SPIE* 3273:134–44
120. Walker RA, Conboy JC, Richmond GL. 1997. *Langmuir* 13:3070–73
121. Smiley BE, Richmond GL. 1999. *J. Phys. Chem.* 103:653–59
122. Huang C, Mason JT. 1986. *Biochim. Biophys. Acta* 864:423–70
123. Smiley BE, Richmond GL. 2000. *Biopolym. Biospectrosc.* 57:111–16